ACS APPLIED MATERIALS & INTERFACES

Subscriber access provided by UNIV OF TEXAS ARLINGTON

Article

Carbon Nanotube Matrix for Highly Sensitive Biosensors to Detect Pancreatic Cancer Biomarker CA19-9

Anshu Thapa, Andrey Coatrini Soares, Juliana Coatrini Soares, Iram Taj Awan, Diogo Volpati, Matias Eliseo Melendez, José Humberto Tavares Guerreiro Fregnani, Andre L. Carvalho, and Osvaldo Novais Oliveira, Jr.

ACS Appl. Mater. Interfaces, **Just Accepted Manuscript** • DOI: 10.1021/acsami.7b07384 • Publication Date (Web): 11 Jul 2017

Downloaded from http://pubs.acs.org on July 12, 2017

Just Accepted

"Just Accepted" manuscripts have been peer-reviewed and accepted for publication. They are posted online prior to technical editing, formatting for publication and author proofing. The American Chemical Society provides "Just Accepted" as a free service to the research community to expedite the dissemination of scientific material as soon as possible after acceptance. "Just Accepted" manuscripts appear in full in PDF format accompanied by an HTML abstract. "Just Accepted" manuscripts have been fully peer reviewed, but should not be considered the official version of record. They are accessible to all readers and citable by the Digital Object Identifier (DOI®). "Just Accepted" is an optional service offered to authors. Therefore, the "Just Accepted" Web site may not include all articles that will be published in the journal. After a manuscript is technically edited and formatted, it will be removed from the "Just Accepted" Web site and published as an ASAP article. Note that technical editing may introduce minor changes to the manuscript text and/or graphics which could affect content, and all legal disclaimers and ethical guidelines that apply to the journal pertain. ACS cannot be held responsible for errors or consequences arising from the use of information contained in these "Just Accepted" manuscripts.

ACS Publications

ACS Applied Materials & Interfaces is published by the American Chemical Society. 1155 Sixteenth Street N.W., Washington, DC 20036

Published by American Chemical Society. Copyright © American Chemical Society. However, no copyright claim is made to original U.S. Government works, or works produced by employees of any Commonwealth realm Crown government in the course of their duties.

Carbon Nanotube Matrix for Highly Sensitive Biosensors to Detect Pancreatic Cancer Biomarker CA19-9

†Anshu Thapa[1,2], †Andrey Coatrini Soares[1], Juliana Coatrini Soares[1], Iram Taj Awan[1], Diogo Volpati[3], Matias Eliseo Melendez[4], José Humberto Tavares Guerreiro Fregnani[4], André Lopes Carvalho[4], *Osvaldo N. Oliveira Jr[1].

[1]São Carlos Institute of Physics, University of São Paulo, São Carlos, Brazil
[2] Department of Physics, University of Bath, Bath, United Kingdom
[3]Mittuniversitetet, Department of Natural Sciences, Sundsvall, Sweden.
[4]Molecular Oncology Research Center, Barretos Cancer Hospital, Barretos, Brazil

Abstract

Biosensors fabricated with nanomaterials promise faster, cheaper and more efficient alternatives to traditional, often bulky, devices for early cancer diagnosis. In this study, we fabricated a thin film sensing unit on interdigitated gold electrodes combining polyethylenemine and carbon nanotubes in a layer by layer fashion, onto which antibodies anti-CA19-9 were adsorbed with a supporting layer of N-hydroxysuccinimide and 1-ethyl-3-(3-dimethylaminopropyl)carbodiimide solution. Using impedance spectroscopy, the pancreatic cancer biomarker CA19-9 was detected in a buffer with limit of detection of 0.35U/mL. This high sensitivity allowed for distinction between samples of blood serum from patients with distinct probabilities to develop pancreatic cancer. The selectivity of the biosensor was confirmed in subsidiary experiments with HT-29 and SW-620 cell lines and possible interferents, e.g. p53 protein, ascorbic acid and glucose, where significant changes in capacitance could only be measured with HT-29 that contained the CA19-9 biomarker. Chemisorption of CA19-9 molecules onto the layer of anti-CA19-9 antibodies was the mechanism responsible for sensing while electrostatic interactions drove the adsorption of carbon nanotubes, according to polarization-modulated infrared reflection absorption spectroscopy (PM-IRRAS). The adsorption behaviour was successfully described by the Langmuir-Freundlich isotherm.

Keywords: cancer, biomarkers, immunosensors, carbon nanotubes, impedance spectroscopy.

1. Introduction

Molecular engineering has been widely exploited to produce biosensors where synergy among constituent materials allows for high sensitivity and selectivity[1,2]. Many examples exist of such devices made in a layer-by-layer fashion with a bioactive layer deposited on a suitable matrix[1,3–6]. The high performance reached by these biosensing systems may be particularly relevant for early cancer diagnosis and prognosis. Indeed, one of the leading causes for the elevated cancer mortality is largely attributed to late stage diagnosis, which sometimes makes subsequent treatment inefficient in controlling the disease. In a research study conducted with 695 patients from 16 acute hospitals of Northern Ireland, it was found that 26.3% of patients were diagnosed with cancer during their last hospital admission, exhibiting more urgent physical symptoms than patients diagnosed at earlier stages[7]. Pancreatic cancer is one of the biggest cancer-killers, with less than 5% survival rate[8,9]. The tumor is often difficult to locate in the body and therefore mostly ever detected in later stages, by which point following treatments become difficult.

A highly robust device, able to diagnose cancer at early stages during routine medical check-up could revolutionize healthcare and potentially reduce cancer related mortality due to late diagnosis. This is motivation for building upon the extensive work already done in biosensors to detect cancer biomarkers[10]. Ideally, a commercial biosensor must be cheap, portable and easy to use, with the single most outstanding feature being its efficiency in detection. One way to successfully achieve high efficiency is by enhancing the sensitivity of the biosensor through surface engineering using nanomaterials. Carbon nanotubes possess a great range of useful physicochemical properties: high conductance, high surface area to volume ratio, surface chemistry and

biocompatibility that make them the ideal choice for use in biosensors whose detection method is based on electrical signal transduction[11,12].

In this study, we used functionalized multi-walled carbon nanotubes (MWCNTs), a concentric bundle of carbon nanotubes, to construct the thin film forming the sensing unit of the biosensor. Covalently functionalized carbon nanotubes form functional groups such as carboxyl[12] on their surface that can be used to chemically attach antibodies on the surface[11]. Because of their hollow shell structure, MWCNTs provide a larger number of sites for binding antibodies in the active layer of the immunosensor, thus potentially yielding a higher sensitivity. The biosensor was designed for the specific detection of carbohydrate antigen 19-9 (CA19-9), a cancer biomarker used for pancreatic cancer diagnosis[9]. The sensing unit of the biosensor was fabricated on an interdigitated gold electrode. A thin film architecture consisting MWCNTs was developed, upon which anti-CA19-9 antibodies were adsorbed for specific binding of CA19-9 antigens present in a given sample solution. The method of signal transduction used was impedance spectroscopy, where the changes measured in capacitance of the sensor upon CA19-9 adsorption was referred as an indication of biomarker detection. The mechanisms driving thin film formation on gold electrodes and antigen-antibody binding were investigated using polarization modulated infrared spectroscopy (PM-IRRAS). In addition to detecting CA19-9 in artificial buffer solutions, the biosensor was employed with whole cell lysates and blood serum of pancreatic cancer patients.

2. Experimental Details

2.1 Fabrication of the sensing unit

The layer-by-layer technique[13,14] was used for constructing a multi-layered film which formed the biosensor. The materials used polyethyleneimine (Sigma-Aldrich, USA), carbon nanotubes (MWCNTs) (Sigma-Aldrich, USA), N-hydroxysuccinimide (NHS) and 1-ethyl-3-(3 dimethylaminopropyl)carbodiimide (EDC) (Sigma-Aldrich, USA), were assembled sequentially on an interdigitated gold electrode surface where a final layer of antibodies anti-CA19-9 (Aviva System Biology, USA) was deposited. The process is illustrated in Figure 1.

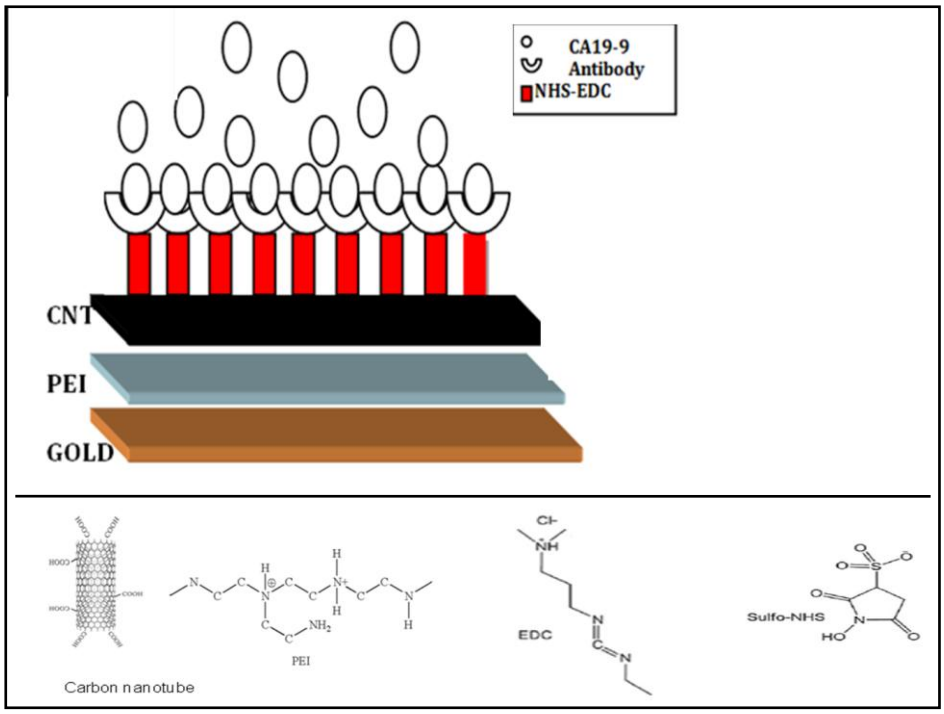

Figure 1: Thin film constructed in a layer-by-layer (LbL) fashion on gold surface using carbon nanotubes (CNTs) and polyethyleneimine (PEI). The carboxylic acid groups on CNTs were activated using NHS-EDC to anchor anti-CA19-9 antibodies on the film surface for specific detection of antigen CA19-9.

The nanostructured films were assembled in the following sequence to create the biosensing unit:

(1) A volume of 20μL polyethyleneimine (PEI) in solution (1mg/mL in water) was adsorbed onto interdigitated gold electrodes deposited on a glass substrate, for an adsorption time of 5 minutes. The electrode was then rinsed with distilled water and dried with a nitrogen gun held at low pressure to remove any unabsorbed molecules from the surface. This insures that any non-specific surface adsorption is avoided.

(2) Then, 20μL of carbon nanotubes (CNTs) were left to adsorb onto the PEI monolayer for 5 minutes and rinsed similarly. Next, 20 μL of N-hydroxysuccinimide (NHS) and 1-ethyl-3-(3-dimethylaminopropyl) carbodiimide (EDC), both at $0.1\ \mathrm{mol}\ L^{-1}$ in water solution, were deposited on the film in equal ratio (1:1). It was left to adsorb on the PEI-CNT film surface for 30 minutes, after which it was rinsed and dried accordingly. Reagents such as NHS and EDC activate the functional carboxylic groups (-COOH) on the carbon nanotube surface. This ensures stable covalent binding between the nanotubes (CNTs) and the antibodies deposited next.

(3) The PEI-CNT-NHS-EDC multi-layered film was lastly coated with a final layer of CA19-9 antibodies with 20μL volume deposition of antibody in phosphate-buffered saline (PBS) solution (1:10) for 45 minutes. Then, the film was rinsed and dried to dispose of any unabsorbed molecules.

The film-fabrication procedure to obtain the biosensor was monitored by taking 1 μm X 1 μm atomic force microscopy (AFM) images with a Bruker dimension FastScan (Bruker Corp., USA) microscope in the tapping mode with a scan rate of 1Hz. Figure 2 shows 3D AFM images, where the most salient feature is the change in root mean square (rms) roughness as the distinct layers are adsorbed. The gold substrate has

a relatively small roughness, which is even decreased by the deposition of the molecularly-thin PEI layer. A large increase in roughness occurs when the CNT layer was adsorbed, which is typical of LbL films of carbon nanotubes. Adsorption of the anti-CA19-9 layer, on the other hand, even led to a decrease in roughness, probably because voids could be filled.

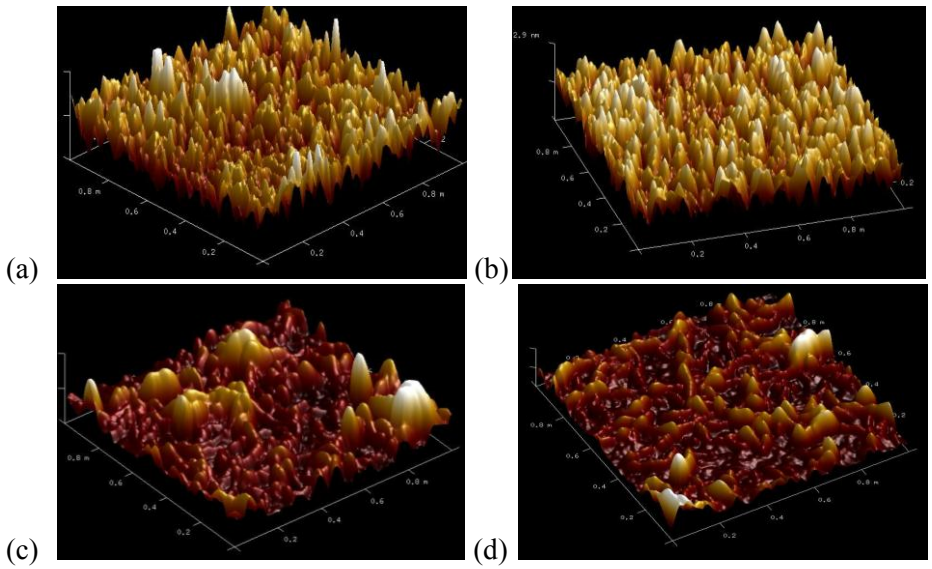

Figure 2: 3-D AFM images showing surface morphology as materials are added layer-by layer in the PEI-CNT film construction. (a) Clean gold surface with roughness 0.943 nm (b) Surface after the deposition of a monolayer of PEI; roughness 0.881 nm (c) Surface after adsorption of CNT; roughness 6.91 nm (d) Surface after adsorption of antibodies (anti-CA19-9); roughness 5.39 nm.

2.2 PM-IRRAS

PM-IRRAS measurements were performed using KSV PMI 550 instrument (Helsinki, Finland) with a spectral resolution of $8cm^{-1}$. A solid gold plate of dimensions 1cm x 1cm was used in place of the gold electrode as the base due to the homogeneity of the gold surface in comparison to interdigitated gold electrodes. After adsorption of each material layer, 1000 measurements were taken using IRRAS 1.0.5 software during

a total time of 300s, the average of which made up the PM-IRRAS signal. Hence, signals measured upon adsorption of each layer were used to characterize the film architecture. Once the nanostructured thin film was characterized, the antibody-antigen interactions of CA19-9 were investigated by taking the gold-PEI-CNT-NHS-EDC film as reference. Various concentrations of CA19-9 antigen (Aviva System Biology, USA) diluted in PBS solution (0, 10, 20, 30, 40, 50, and 60 U/mL) were used. An antigen volume of 80μL was deposited on the film surface and left to adsorb for 10 minutes, after which it was rinsed with distilled water and dried before taking measurements.

2.3 Impedance Spectroscopy as a Method of Detection

Electrical impedance measurements were performed using a Solartron 1260A impedance/gain phase analyser (Solartron, Farnborough, England) with an applied AC voltage of 50mV. The sensing unit was fabricated on 50 pairs of interdigitated gold electrodes with separation and width dimension of 10μm as described by Soares et al[3]. The capacitance values were taken over the frequency range of 1 -10^6 Hz, recorded with the Software packages ZView 2 and ZPlot 2. The sensing units fabricated following the method described in section 2.1 were exposed to samples containing various concentrations of CA19-9 antigen diluted in 20μL PBS solution, pH 7.4. The CA19-9 concentrated sample solutions (0, 0.05, 0.5, 1, 4, 8, 20, 40, and 60U/mL) were deposited onto the sensing units and were left to adsorb for 10 minutes, after which they were washed with distilled water and dried. In addition, whole cell lysates obtained from Barretos Cancer Hospital as well as solutions of glucose (Sigma-Aldrich), ascorbic acid (Sigma-Aldrich) and p53 biomarker (ABCAM) were tested. Whole cell lysates of colorectal adenocarcinoma HT-29 (CA19-9 expressing) and SW-620 (CA19-9 null) cell

lines were obtained by three cycles of freeze–thaw and stored at -80ºC. HT-29 (ATCC) and SW-620 (ATCC) cell lines were maintained in Dulbecco's modified eagle's medium (DMEM), containing 10% fetal bovine serum (FBS), 2 mM glutamine, 1% penicillin/streptomycin, in a humidified CO2 incubator at 37 °C. Confluent cell lines were washed with PBS and cultured in OptiMEM media, without serum supplementation. After 48 hours of incubation, supernatants were filtered through a 0.22 μm filter and stored at −80°C until analysis. Glucose (100mg/dL in distilled water solution), ascorbic acid (4.8mg/mL in distilled water) and antigen p53 (5ng/mL in PBS solution) were considered negative controls and therefore used in investigating the specificity of the sensor.

2.4 Data Analysis

Information visualization techniques are being used to analyze the large amounts of data in the fields of sensors and biosensors[1,2,15,16]. The capacitance vs. frequency data obtained via Impedance Spectroscopy has a high dimensionality for a given sample. For measurements taken over multiple samples, it becomes nearly impossible to extract any useful information. A multidimensional projection technique converts the information held within each high dimensional data instance into a format where it is possible to see the global similarity relationships amongst the data instances. The principle of this technique is based on dimensionality reduction while preserving similarity relationships, so that similar data is placed as close to each other as possible on the projected space[15]. This technique, implemented in free software referred to as PEx-Sensors, was used to represent the high-dimensional spectra of capacitance vs. frequency measurements obtained via impedance spectroscopy. It considers the

Euclidean distance between two spectra of data, X_i and X_j, with each spectrum consisting of capacitance values $X = \{x_1, x_2, \ldots, x_n\}$. A set of graphical markers represented by the vector $Y = \{y_1, y_{2,\ldots,} y_n\}$, whose Euclidean distance between data instances is denoted by $d(y_i - y_j)$, is projected onto a 2D space using an injective function $f: X \rightarrow Y$ that attempts to minimize the so-called cost or error function, $|\delta(x_i, x_j) - d(yi - y_j)|$for $\forall x_i, x_j \in$ X[16]. Non-linear mapping such as Interactive Document Map (IDMAP) has been shown to be the best strategy for biosensor data representation in the literature[1,3,4,15]. IDMAP is a multidimensional projection technique that uses force minimization approach to place two data points together in 2-D space using the following function [15,17]:

$$\Delta = \frac{\delta(X_i, X_j) - \delta_{min}}{\delta_{max} - \delta_{min}} - d(Y_i, Y_j) \quad (1)$$

where δ_{min} is the minimum distance and δ_{max} is the maximum distance of the spectrum measured in the original space. This ensures that the dissimilarities in spectra of the data collected are accurately represented on IDMAP as points.

2.5. Assay Validation in Real Samples

Cell line supernatants and serum samples from cancer patients were previously quantified using the electrochemiluminescence analyzer model Cobas 601 (Roche Diagnostics, Indianapolis) and an Elecsys CA 19-9 Immunoassay kit (Roche Diagnostics, Indianapolis). The use of patient serum samples was approved by the Ethics Committees in Research of Barretos Cancer Hospital and Federal University of São Carlos.

3. Results and Discussion

3.1 Detection of cancer biomarker

The PEI-CNT biosensor could successfully detect and distinguish between the different concentrations of CA19-9 biomarkers diluted in PBS solutions. Figure 3 shows the capacitance vs. frequency data acquired for various CA19-9 concentrations over the frequency range 1 to 10^6 Hz. The capacitance curve at 0U/ml represents the capacitance profile of the (blank) sensor without CA19-9 biomarkers adsorbed. The adsorption of biomarkers induces changes in electrical response of the sensor that can be measured in terms of capacitance. At high frequencies ($>10^5$Hz), the electrical response is dominated by the electrode geometry[18], which is the same regardless of the amount of CA19-9 biomarkers adsorbed. In the mid-range frequency (100Hz-1 kHz) the amount of CA19-9 antigen adsorbed on the film determines the capacitive ability of the electrode, which increases with concentration. A clear distinction between the different concentrations observed in Figure 3(a) between 100-1000Hz frequencies suggests the sensor is most sensitive in this region. In the low frequency regime (<100Hz) electrostatically driven double layer effects at the film surface are observed and are not entirely concentration dependent.

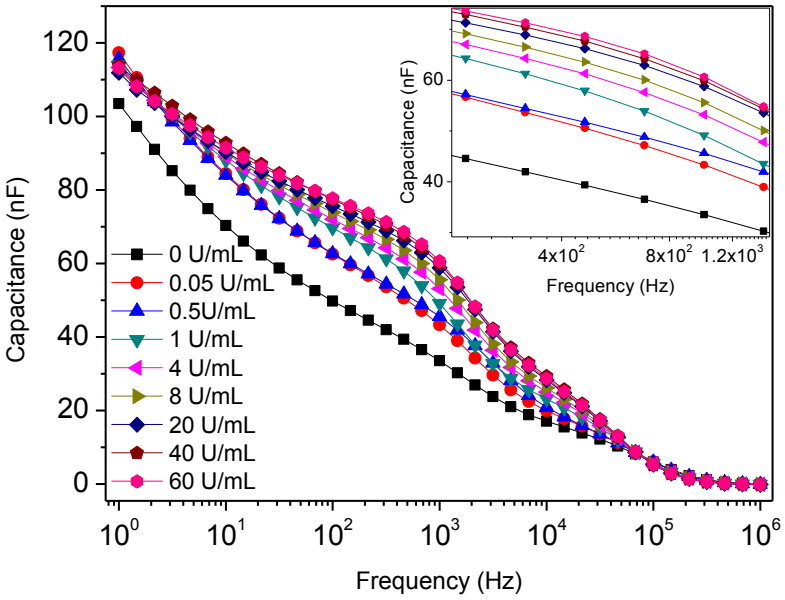

Figure 3: Capacitance versus Frequency spectrum for electrodes modified with PEI-MWCNT films, immersed in PBS solution with different CA19-9 concentrations. The insert shows the data focused between 100 and 1000 Hz.

In order to represent the dissimilarity between concentrations, the capacitance vs. frequency spectra were treated with IDMAP technique in PEx-Sensors software, as shown in Figure 4a. The IDMAP represents each sample as points on a label-less 2D map, which are placed close to each other when the capacitance spectra are similar. Note, therefore, that the axes are not labelled because there is no physical meaning for the horizontal and vertical axis; what matters is the relative distance between data points. The data plotted visually represents the distinction between behavior of the sensor at low concentration region (0.05U/mL, 0.5U/ml) and high concentration region (40U/mL - 60U/mL) upon CA19-9 biomarker adsorption. The dissimilarity in data points for the concentrations used proves distinguishability of the biosensor and hence its reliability in clinical diagnosis.

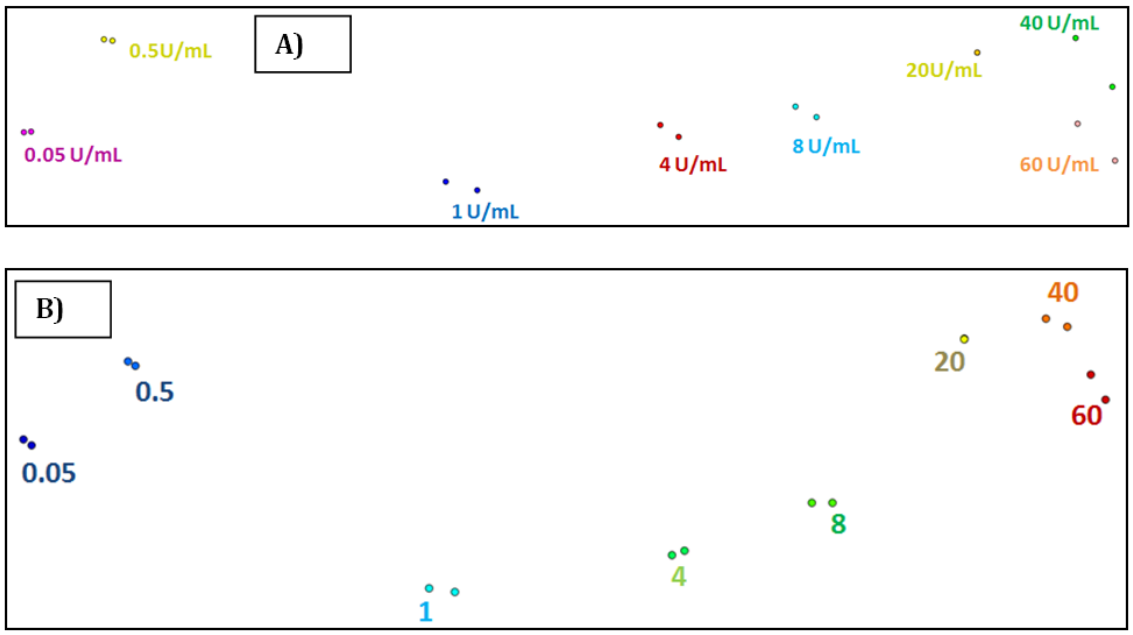

Figure 4: (a) IDMAP of capacitance vs. frequency data of CA19-9 biomarker diluted in PBS solution. (b) IDMAP of capacitance x frequency data of CA19-9 biomarker for 10 selected frequencies. Each dot represents the spectrum for the corresponding concentration. The axes are not labelled because what matters in the plot is the relative distance between data points.

One figure of merit relevant for any immunosensor is the limit of detection, normally determined from a calibration curve. A visual representation such as that provided by IDMAP is not suitable for generating a calibration curve, and this can be done by choosing a fixed frequency to analyze the capacitance data. In order to be quantitative, we plotted the capacitance spectra using the Parallel Coordinates technique[19] in Figure 5, with which one may calculate the silhouette coefficient (S)[15,16] that is a measure of the distinguishing ability of different instances in a dataset. This coefficient S varies between -1 and 1, where values close to 1 mean that using the corresponding data is useful for discrimination, values close to -1 are deleterious and values close to 0 are neutral with regard to discrimination. On the top of the plot in Figure 5 the blue boxes represent frequencies with high S, the white boxes represent S ~ 0 and the red box represents a frequency with S close to -1. If all the frequencies measured (61) are used, the overall S is 0.78, thus reflecting the large number of blue

boxes on the plot. When only the 10 selected frequencies that yield good distinction are used, S increases to 0.902. The improvement can be visualized in the IDMAP plot of Figure 4(b). Also relevant is that the region of intermediate frequencies is ideal for discrimination of the CA19-9 commercial samples with various concentrations, from which we chose 1 kHz for obtaining the calibration curve (see below).

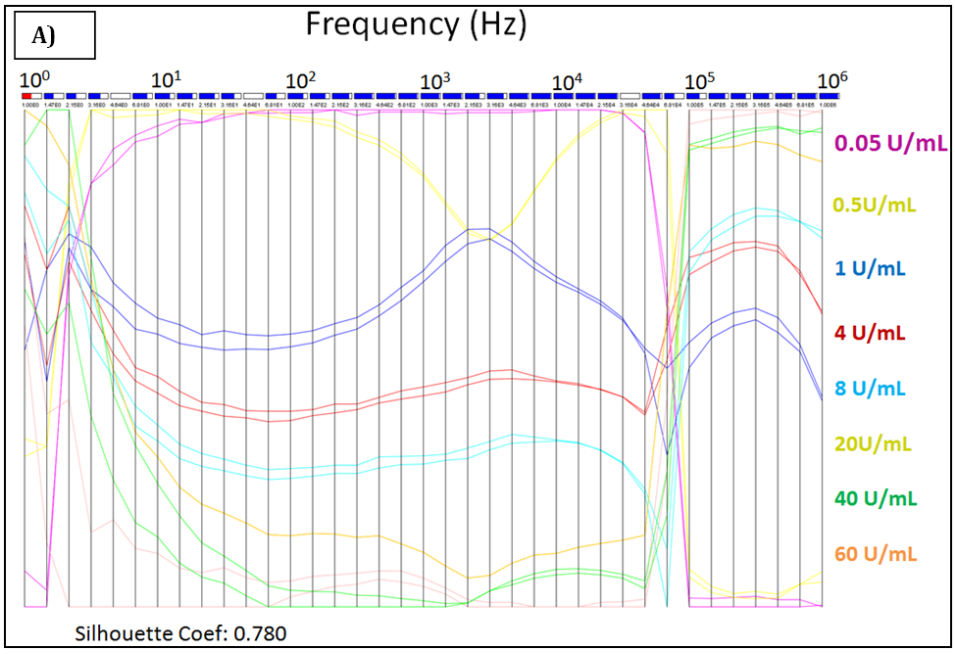

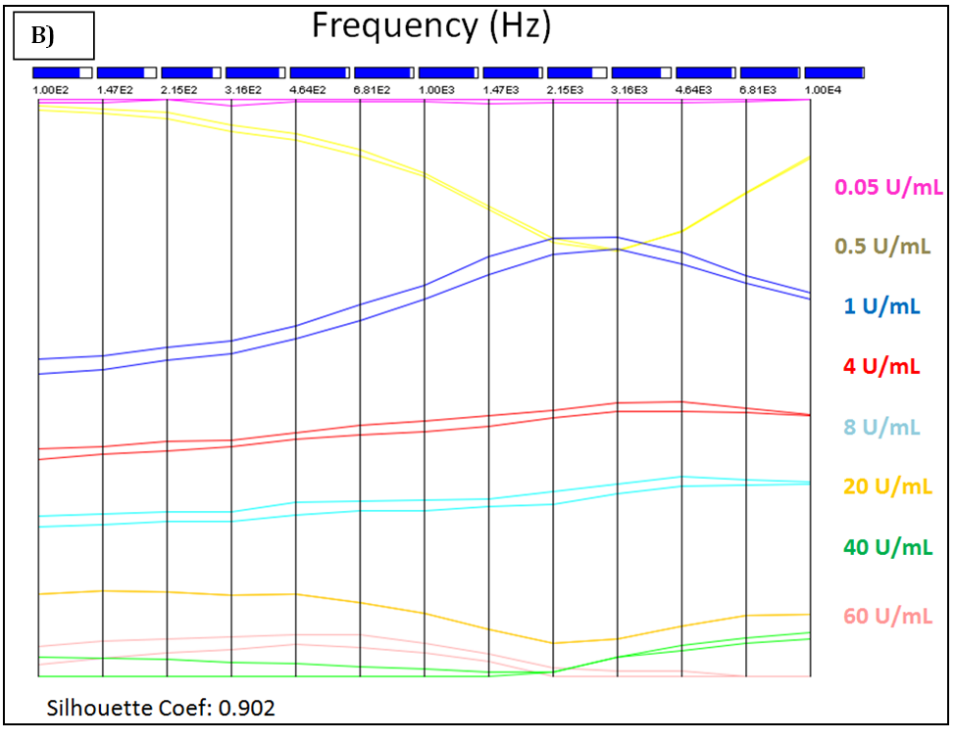

Figure 5: (a) Parallel coordinates graph obtained from capacitance x frequency spectra of different CA19-9 concentrations in commercial samples. (b) Parallel coordinates graph obtained from capacitance x frequency spectra for 10 selected frequencies. The x-axis corresponds to the frequency while the y-axis brings normalized capacitance values. The blue boxes indicate that the region of intermediate frequencies, between 100-10000 Hz, is more suitable to distinguish the samples.

From the analysis above with calculation of silhouette coefficients, we inferred that 1 kHz is one of the most useful frequencies in distinguishing the samples. We have therefore used the capacitance at 1 kHz from Figure 3 to plot the calibration curve of Figure 6, where the reference is the capacitance measured with the PBS buffer. The curve can be fitted with a Langmuir-Freundlich isotherm[20,21] in Eq. (2), which seems a typical behaviour for antigen-antibody adsorption in immunosensors:

$$q = \frac{Q_{sat}.k.c^n}{1+(k.c^n)} \quad (2)$$

where q is the amount of CA19-9 adsorbed on the film at equilibrium; Q_{sat} is the absorption capacity of the system; k is the affinity constant for adsorption; c is the aqueous phase concentration of CA19-9 and n is the heterogeneity index. The index n is a measure of surface heterogeneity, which has a value between 0 and 1, where 1 indicates a homogeneity[21]. An index n = 0.257 suggests that the final surface layer, made up of adsorbed CA19-9 biomarkers, was not homogenous. This is likely due to some excess molecules that remained after washing, forming weak electrostatic bonds with the adsorbed molecules. Note that in fitting with the Langmuir-Freundlich isotherm we assume that the change in capacitance is proportional to the amount of material adsorbed. The value of Q_{sat} thus represents the saturation capacitance value which, by extrapolation of Figure 6, occurs beyond 60 U/mL. In clinical diagnosis, 37U/mL is the standard benchmark concentration used to identify cancer positives

(>37U/mL) from cancer negatives (<37U/mL) in blood samples. As saturation concentration is beyond this number, the sensor can distinguish concentrations well below and above the benchmark concentration, which renders a promising application of the sensor in clinical diagnosis

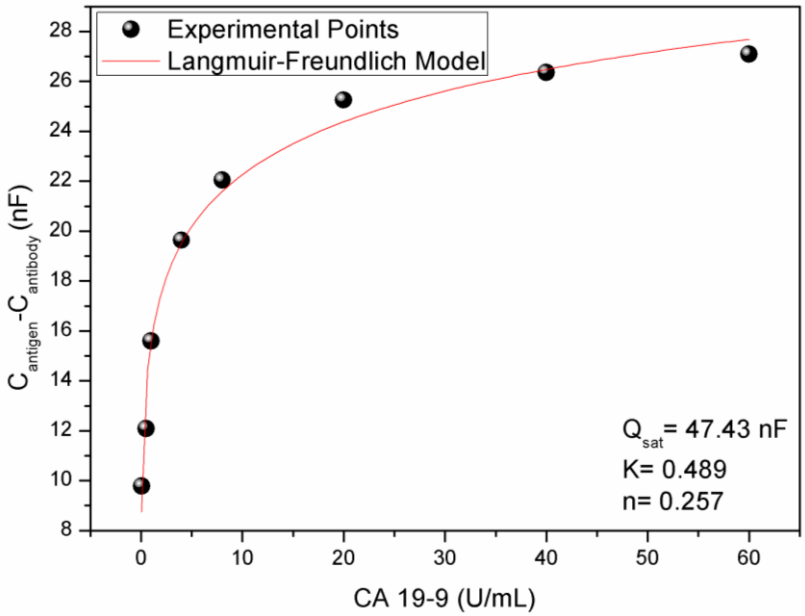

Figure 6: Relative capacitance showing capacitance change upon adsorption of CA19-9. The adsorption behaviour is modelled by a Langmuir-Freundlich isotherm (solid line).

The sensitivity of the PEI-CNT biosensor was estimated by calculating the lowest amount of CA19-9 antigen that could be detected, i.e. the limit of detection (LD) using the IUPAC method[3,22]:

$$LD = \frac{3 \times SD}{slope} \quad (3)$$

where *SD* refers to standard deviation and *slope* refers to the gradient of the calibration graph. The limit of detection was calculated graphically from the calibration curve in Figure 6 by considering the steep slope encompassing the first three data points. Using eq. (3), the limit of detection was deduced to be 0.35U/mL, which is configured as the

lowest level of CA19-9 concentration that the biosensor is capable of detecting. This limit of detection is among the lowest reported in the literature; it is lower than the values for commercial sensors Architect i2000 (2 U/mL), AxSYM (2 U/mL), KRYPTOR (1,2 U/mL), Elecsys (0.6 U/mL)[23] and competitive with similar biosensors made with nanostructured films: 0.69 U/mL for chitosan/Con A matrix[1], 0.01 U/mL for nanostructured films made with Au–SiO_2/Fe_3O_4 nanospheres[24] and 0.006 U/mL[25] for sensors made with Au/porous graphene nanocomposites matrix.

With its high sensitivity, we could test the PEI-CNT immunosensor with real samples taken from cell lysates and blood serum from patients, in addition to verifying the robustness in the performance with regard to selectivity. The IDMAP plot in Figure 7 obtained from capacitance data does indicate that the real samples HT-29 (CA19-9 positive) and SW-620 (CA19-9 negative) can be distinguished from each other. Furthermore, the data for interferents were placed far from those of commercial samples containing the various CA19-9 concentrations, perhaps with the exception of the cancer biomarker p53, which is nevertheless close to the data points for the very small CA19-9 concentrations. Therefore, this plot demonstrates that the immunosensor can be selective for CA19-9-positive cells and does not suffer from interference of other analytes that may be present in biological fluids. The immunosensor only produces recognizable signals due to CA19-9 biomarker adsorption.

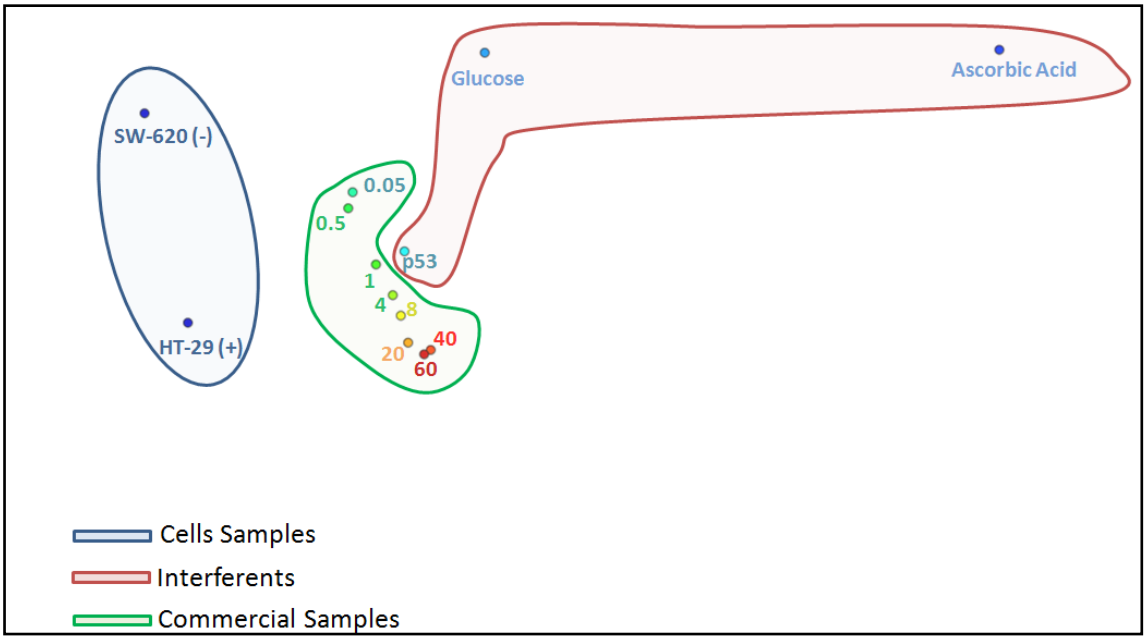

Figure 7: IDMAP of capacitance x frequency spectra of two supernatants cells samples HT-29 and SW-620 (blue region), three interferents (red region) and commercial samples (green region), indicating absence of false positives and the presence of CA 19-9 in HT-29 cell supernatants. As in Figure 4, the axes are not labelled.

An even more challenging task is to detect CA19-9 in blood serum from patients. The IDMAP plot obtained from the capacitance data in Figure 8 indicates excellent distinction between blood serum samples from 5 patients from Barretos Cancer Hospital (Ethics Committee number 1.447.041, Brazil). Significantly, the distance along the y-axis in the plot correlates with CA19-9 concentration, and there is clustering of samples in two distinct regions. Hence, the immunosensor made with PEI/CNT nanostructured films is able to distinguish between patients with high concentration level of CA 19-9 and those with low concentration level of CA19-9.

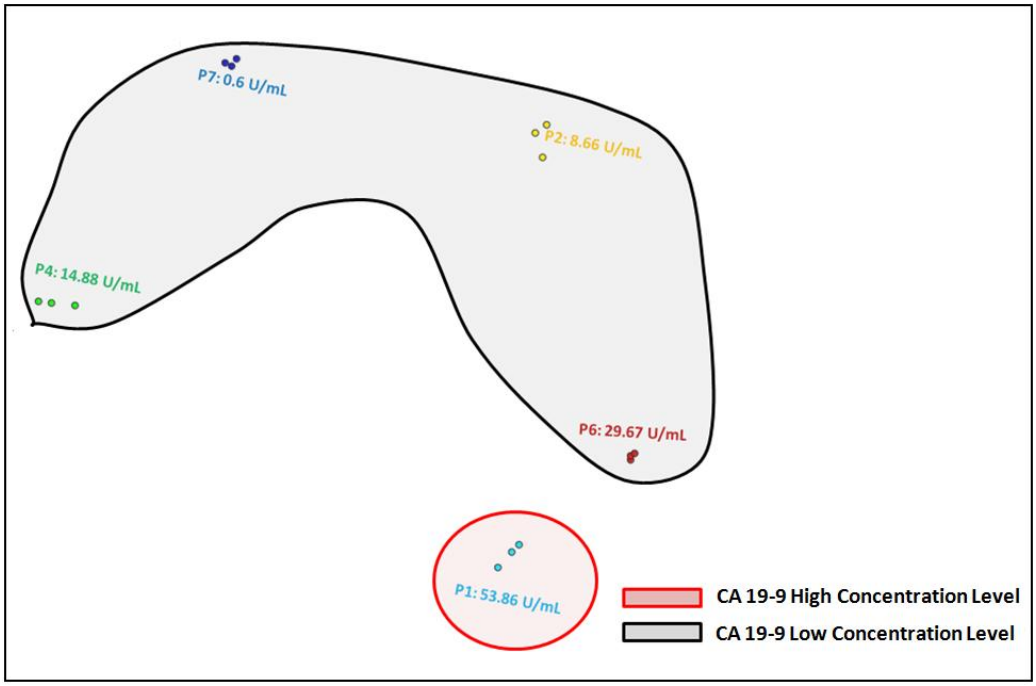

Figure 8: IDMAP obtained from the capacitance x frequency curves of 5 serum samples from patients from Barretos Cancer Hospital (Ethics Committee number 1.447.041, Brazil). As in Figures 4 and 7 the axes are not labelled.

3.2 Adsorption Mechanism Behind Biosensing

The mechanism that enables the high sensitivity is thought to be chemical binding between CA19-9 antigen and the antibody anti-CA19-9. Further studies using polarization modulation infrared spectroscopy technique were conducted to identify the mechanisms involved in adsorption. The infrared absorption spectra using the PM-IRRAS technique revealed changes in surface chemistry of the gold electrode upon adsorption of materials constituting the film. The signal observed upon adsorption of polyethyleneimine (PEI) and carbon nanotubes (CNT) adsorption on a gold plate is shown in Figure 9, where the baseline correction was made by taking the spectrum of blank gold surface as reference. PEI is largely composed of amine groups, which contain nitrogen atoms bonded to hydrogen (NH bonds) and are responsible for the strong bands in Figure 9a (PEI). The vibrational broad band around $1530\,cm^{-1}$ is

assigned to NH deformation[26] in amines. Stretching vibrations of the *C-N* group in amide I create the broadband at 1403 cm^{-1} [26]. *C-N* amine vibration is also responsible for the band around 1323 cm [26]. Carbon nanotubes (CNTs) were covalently functionalized with carboxylic groups tethered on their surface. The vibrational bands observed in Figure 9c (CNT) are associated with the vibrations of carbonyl and hydroxyl groups. The narrow broadband at $1350\ cm^{-1}$ is due to in-plane OH bending of the C-OH hydroxyl group[26] C=O carbonyl stretching is associated with the vibration at $1714\ cm^{-1}$ and sp^2-hybridized C=C in-plane vibration is associated with $1665\ cm^{-1}$ [26]. The PM-IRRAS spectrum in Figure 9b (CNT + PEI) after sequential adsorption of PEI and CNT (PEI+CNT) is a superposition of the independent spectra of polyethyleneimine (PEI) and carbon nanotubes (CNT). No apparent shift in wavenumber is observed upon adsorption of carbon nanotubes (CNT) on polyethyleneimine (PEI) layer, which indicates the adsorption of CNT on PEI layer is not driven by chemisorption since chemical bonding changes molecular structure on the surface and produces shifts of vibrational wavenumber[27]. Hence, the type of adsorption taking place in thin film construction are the electrostatic and/or van der Waals interactions between the two layers of material.

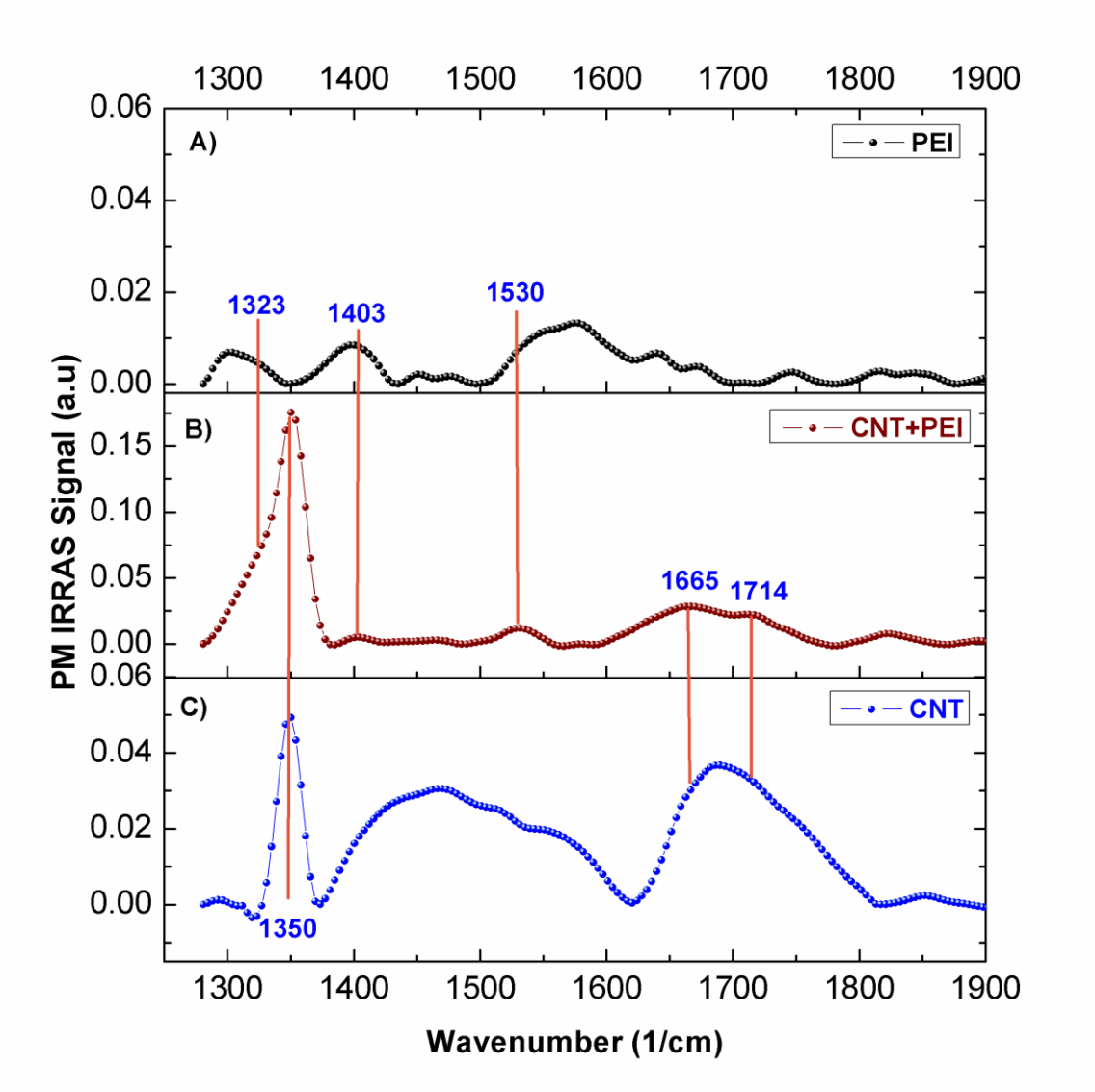

Figure 9: PM-IRRAS signal of the PEI-CNT biosensor in (1300-1900)cm^{-1} infrared frequency region.

Infrared reflection adsorption spectra provide unique means of studying protein conformation in films[27]. The adsorption of CA19-9 antigen on the PEI-CNT film immobilized with antibodies (anti-CA19-9) was studied using the PM-IRRAS technique whose structural information was extracted from spectral analysis. It is generally hard to establish all the molecular constituents responsible for vibration peaks due to the complex nature of peptides and proteins[27]. However, from known correlation spectra of small molecules, information about the molecular interaction between anti-CA19-9 and

CA19-9 antigen could be extrapolated. The data acquired have been corrected taking the spectrum of a PEI/MWCNT/EDC/NHS film as baseline. The vibrational band at $3500 cm^{-1}$ for 0U/mL in Figure 10(a) is associated with NH stretching of primary amides[28] attached to the antibody (anti-CA19-9) protein chains. The first layer of CA19-9 antigen adsorption (10U/mL) causes the NH vibrational band to shift (increasing wavenumber) and the peak intensity to decrease. The shifts observed with antigen adsorption indicate change in molecular structure of the blank (containing antibody only) film, which suggests chemisorption to be the principal mechanism of interaction between antibodies and antigen. Shifts are also observed for the peaks in Figure 10(b), where spectra obtained with higher CA19-9 concentrations are shown.

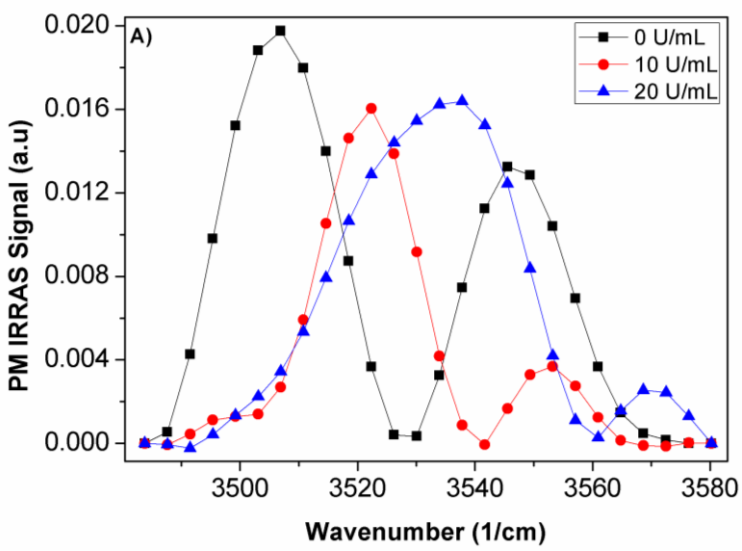

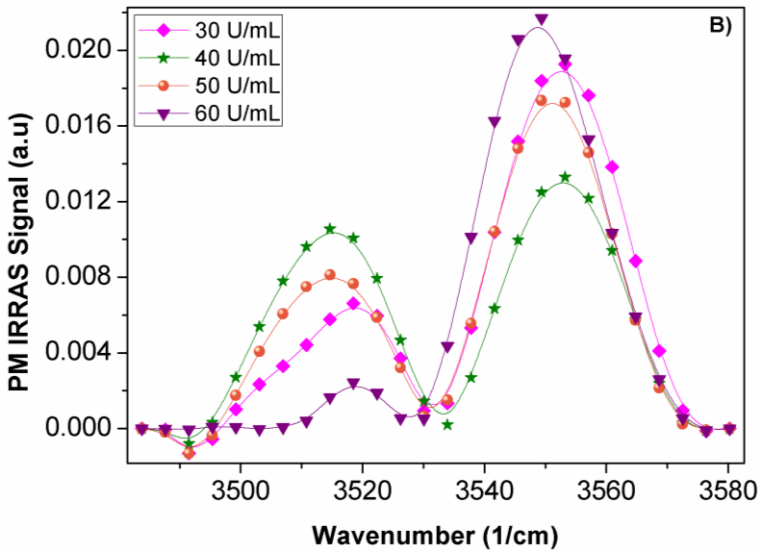

Figure 10: PM IRRAS spectra of adsorption CA 19-9 biomarkers in active layer immobilized in carbon nanotubes matrix: (a) Spectra between 0-20 U/mL (b) Spectra between 30 and 60 U/mL.

A pictorial view of the sensing mechanism can be drawn based on the PM-IRRAS data. The biosensor architecture of Figure 11 is shown to illustrate that adsorption only occurs when the antigen CA19-9 finds its corresponding antibody, as inferred from the selectivity studies. The zoomed figure depicts the H-bonding interaction of the NH_2 group of the antibody and the C = O[29] group of the antigen, which is inferred from the changes in the PM-IRRAS spectra.

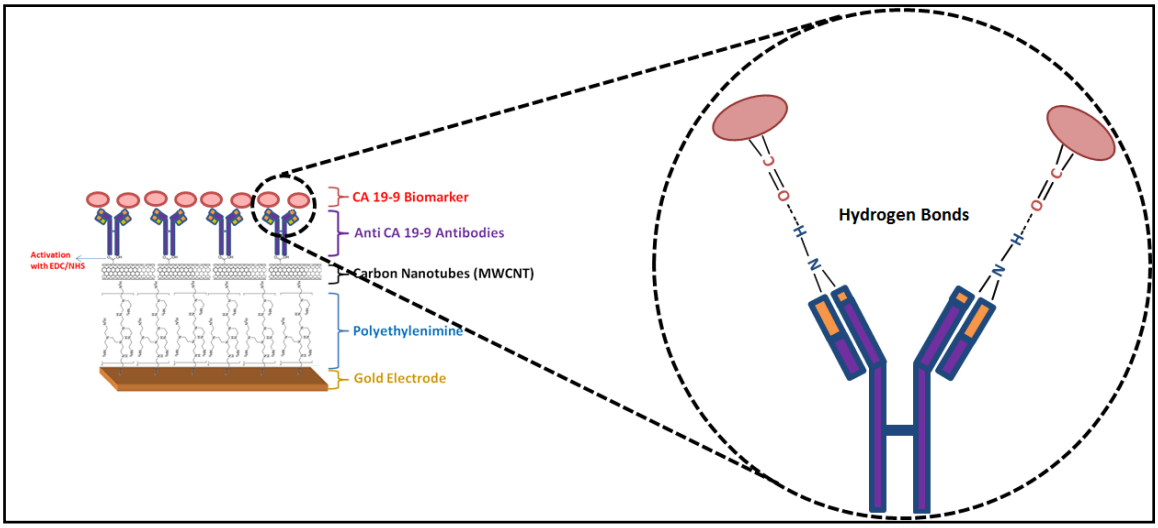

Figure 11: The figure depicts schematically the interactions taking place between antibodies and antigens, which are responsible for the sensing mechanisms. The whole architecture of the biosensor is represented. Specificity of the antigen-antibody interactions is warranted by the surface shape of the topmost layer containing the anti-CA19-9 antibodies. In the zoomed figure, H-bonds are shown which lead to shifts in NH and amide bands in the PM-IRRAS spectra.

4. Conclusion.

A sensitive biosensor made with a matrix of PEI-CNT coated with a layer of anti-CA19-9 antibodies has been produced which can specifically detect cancer biomarker CA19-9 using impedance spectroscopy with a detection limit of 0.35U/mL. Several tests conducted with samples containing glucose, ascorbic acid and p53 antigen confirmed that the biosensor is only selective to CA19-9 biomarker. Using multidimensional projection techniques implemented in PEx-Sensors software, the biosensor's ability to clearly distinguish between samples with and without CA19-9 biomarkers was also established. Significantly, it was possible to discriminate samples of blood serum from patients with distinct probabilities to develop pancreatic cancer. An analytical interpretation of the capacitance change with concentration revealed that the CA19-9 adsorption on PEI-CNT biosensor could be described by a Langmuir-Freundlich isotherm.

The study of surface adsorption on film using PM-IRRAS revealed the mechanisms driving adsorption. It was found that electrostatic and van der Waals interactions were responsible for material adsorption during PEI-CNT thin film fabrication while chemical bonding was responsible for CA19-9 antigen adsorption on the sensor surface. Functional groups were identified according to vibrational signals produced with PM-IRRAS, which showed signal changes upon CA19-9 adsorption. This indicates that these functional groups are crucial in molecular interaction between CA19-9 antigen and antibody. As chemical interaction is responsible for CA19-9 adsorption, further studies can focus on manipulating the molecular recognition element of the sensor by studying the PM-IRRAS results presented in this paper. In this way, biosensors with higher specificity and sensitivity can be designed in the future for early detections of cancer. Such robust biosensors could revolutionize clinical diagnosis by even eliminating the need for blood samples in cancer detection and instead make use of bodily fluid such as saliva. Salivation detection method is non-invasive and could reduce cost and time involved in cancer diagnosis. The experimental procedure outlined here could be followed with biomarkers diluted in artificial saliva to test the sensor's effectiveness in biomarker detection.

5. Author Information

Corresponding Author

*E-mail: chu@ifsc.usp.br

Author Contributions

†Anshu Thapa and Andrey Coatrini Soares contributed equally to this work.

6. Acknowledgements.

This work was supported by CNPq, FAPESP (2013/14262-7) (Brazil) and Barretos Cancer Hospital. The authors are also grateful to Angelo L. Gobbi and Maria H. O. Piazzetta for use of LNNANO Microfabrication Laboratory (LMF/LNNANO/CNPEM).

7. References.

(1) Soares, A. C.; Soares, J. C.; Shimizu, F. M.; Melendez, M. E.; Carvalho, A. L.; Oliveira, O. N. Controlled Film Architectures to Detect a Biomarker for Pancreatic Cancer Using Impedance Spectroscopy. *ACS Appl. Mater. Interfaces* **2015**, *7*, 25930–25937.

(2) Oliveira, O. N.; Iost, R. M.; Siqueira, J. R.; Crespilho, F. N.; Caseli, L. Nanomaterials for Diagnosis: Challenges and Applications in Smart Devices Based on Molecular Recognition. *ACS Appl. Mater. Interfaces* **2014**, *6*, 14745–14766.

(3) Soares, J. C.; Shimizu, F. M.; Soares, A. C.; Caseli, L.; Ferreira, J.; Oliveira, O. N. Supramolecular Control in Nanostructured Film Architectures for Detecting Breast Cancer. *ACS Appl. Mater. Interfaces* **2015**, *7*, 11833–11841.

(4) Soares, J. C.; Soares, A. C.; Pereira, P. A. R.; Rodrigues, V. da C.; Shimizu, F. M.; Melendez, M. E.; Scapulatempo Neto, C.; Carvalho, A. L.; Leite, F. L.; Machado, S. A. S.; Oliveira, O. N. Adsorption according to the Langmuir–Freundlich Model Is the Detection Mechanism of the Antigen p53 for Early Diagnosis of Cancer. *Phys Chem Chem Phys* **2016**, *18*, 8412–8418.

(5) Raymundo-Pereira, P. A.; Shimizu, F. M.; Coelho, D.; Piazzeta, M. H. O.; Gobbi, A. L.; Machado, S. A. S.; Oliveira, O. N. A Nanostructured Bifunctional Platform for Sensing of Glucose Biomarker in Artificial Saliva: Synergy in Hybrid Pt/Au Surfaces. *Biosens. Bioelectron.* **2016**, *86*, 369–376.

(6) Moraes, M. L.; Rodrigues, V. C.; Soares, J. C.; Ferreira, M.; de Souza, N. C.; Oliveira, O. N. Immunosensor for HIV-1 Diagnostics Based on Immobilization of the Antigenic Peptide p24-3 into Liposomes. *J. Nanosci. Nanotechnol.* **2014**, *14*, 6638–6645.

(7) Blaney, J.; Crawford, G.; Elder, T.; Johnston, G.; Gavin, A. Hospital Cancer Deaths: Late Diagnosis and Missed Opportunity. *BMJ Support. Palliat. Care* **2011**, *1*, 135–139.

(8) Ballehaninna, U. K.; Chamberlain, R. S. Serum CA 19-9 as a Biomarker for Pancreatic Cancer—A Comprehensive Review. *Indian J. Surg. Oncol.* **2011**, *2*, 88–100.

(9) International Agency for Research on Cancer. The Pancreatic Cancer Working Group, http://epic.iarc.fr/research/cancerworkinggroups/pancreaticcancer.php. (accessed on Nov. 20, 2016)

(10) Vigneshvar, S.; Sudhakumari, C. C.; Senthilkumaran, B.; Prakash, H. Recent Advances in Biosensor Technology for Potential Applications – An Overview. *Front. Bioeng. Biotechnol.* **2016**, *4,* Article 11 (9pp).

(11) Sharma, P.; Mehra, N. K.; Jain, K.; Jain, N. K. Biomedical Applications of Carbon Nanotubes: A Critical Review. *Curr. Drug Deliv.* **2016**, *13*, 796–817.

(12) Yang, N.; Chen, X.; Ren, T.; Zhang, P.; Yang, D. Carbon Nanotube Based Biosensors. *Sens. Actuators B Chem.* **2015**, *207*, 690–715.

(13) Ariga, K.; Yamauchi, Y.; Rydzek, G.; Ji, Q.; Yonamine, Y.; Wu, K. C.-W.; Hill, J. P. Layer-by-Layer Nanoarchitectonics: Invention, Innovation, and Evolution. *Chem. Lett.* **2014**, *43*, 36–68.

(14) Rydzek, G.; Ji, Q.; Li, M.; Schaaf, P.; Hill, J. P.; Boulmedais, F.; Ariga, K. Electrochemical Nanoarchitectonics and Layer-by-Layer Assembly: From Basics to Future. *Nano Today* **2015**, *10*, 138–167.

(15) Oliveira, O. N.; Pavinatto, F. J.; Constantino, C. J. L.; Paulovich, F. V.; de Oliveira, M. C. F. Information Visualization to Enhance Sensitivity and Selectivity in Biosensing. *Biointerphases* **2012**, *7*, 1-15.

(16) Paulovich, F. V.; Moraes, M. L.; Maki, R. M.; Ferreira, M.; Oliveira Jr., O. N.; de Oliveira, M. C. F. Information Visualization Techniques for Sensing and Biosensing. *The Analyst* **2011**, *136*, 1344-1350.

(17) Oliveira, Jr., O. N.; Neves, T. T. A. T.; Paulovich, F. V.; de Oliveira, M. C. F. Where Chemical Sensors May Assist in Clinical Diagnosis Exploring "Big Data." *Chem. Lett.* **2014**, *43*, 1672–1679.

(18) Lvovich, V. F. *Impedance Spectroscopy: Applications to Electrochemical and Dielectric Phenomena*; Wiley: Hoboken, N.J, 2012.

(19) Inselberg, A.; Dimsdale, B. Parallel Coordinates: A Tool for Visualizing Multi-Dimensional Geometry. *Proc. First IEEE Conf. Vis* **1990**, 361–378.

(20) Jeppu, G. P.; Clement, T. P. A Modified Langmuir-Freundlich Isotherm Model for Simulating pH-Dependent Adsorption Effects. *J. Contam. Hydrol.* **2012**, *129–130*, 46–53.

(21) Turiel, E.; Perez-Conde, C.; Martin-Esteban, A. Assessment of the Cross-Reactivity and Binding Sites Characterisation of a Propazine-Imprinted Polymer Using the Langmuir-Freundlich Isotherm. *The Analyst* **2003**, *128*, 137–141.

(22) Rodrigues, V. da C.; Comin, C. H.; Soares, J. C.; Soares, A. C.; Melendez, M. E.; Fregnani, J. H. T. G.; Carvalho, A. L.; Costa, L. da F.; Oliveira, O. N. Analysis of Scanning Electron Microscopy Images To Investigate Adsorption Processes Responsible for Detection of Cancer Biomarkers. *ACS Appl. Mater. Interfaces* **2017**, *9*, 5885–5890.

(23) Passerini, R.; Riggio, D.; Salvatici, M.; Zorzino, L.; Radice, D.; Sandri, M. T. Interchangeability of Measurements of CA 19-9 in Serum with Four Frequently Used Assays: An Update. *Clin. Chem. Lab. Med.* **2007**, *45*, 100-104.

(24) Zhang, Q.; Chen, X.; Tang, Y.; Ge, L.; Guo, B.; Yao, C. Amperometric Carbohydrate Antigen 19-9 Immunosensor Based on Three Dimensional Ordered Macroporous Magnetic Au Film Coupling Direct Electrochemistry of Horseradish Peroxidase. *Anal. Chim. Acta* **2014**, *815*, 42–50.

(25) Yang, F.; Yang, Z.; Zhuo, Y.; Chai, Y.; Yuan, R. Ultrasensitive Electrochemical Immunosensor for Carbohydrate Antigen 19-9 Using Au/Porous Graphene Nanocomposites as Platform and Au@Pd Core/Shell Bimetallic Functionalized Graphene Nanocomposites as Signal Enhancers. *Biosens. Bioelectron.* **2015**, *66*, 356–362.

(26) Lambert, J. B. *Introduction to Organic Spectroscopy*; Macmillan: New York, 1987.

(27) Barth, A. Infrared Spectroscopy of Proteins. *Biochim. Biophys. Acta BBA - Bioenerg.* **2007**, *1767*, 1073–1101.

(28) Krueger, P. J. Fundamental NH2 Stretching Frequencies in Amines and Amides. *Nature* **1962**, *194*, 1077–1078.

(29) Murphy, K.; Travers, P.; Walport, M. *Janneway's Immunobiology.* Garland Science: New York, 2008

Carbon Nanotube Matrix for Highly Sensitive Biosensors to Detect Pancreatic Cancer Biomarker CA19-9

†Anshu Thapa[1,2], †Andrey Coatrini Soares[1], Juliana Coatrini Soares[1], Iram Taj Awan[1], Diogo Volpati[3], Matias Eliseo Melendez[4], José Humberto Tavares Guerreiro Fregnani[4], André Lopes Carvalho[4], *Osvaldo N. Oliveira Jr[1].

[1]São Carlos Institute of Physics, University of São Paulo, São Carlos, Brazil
[2] Department of Physics, University of Bath, Bath, United Kingdom
[3]Mittuniversitetet, Department of Natural Sciences, Sundsvall, Sweden.
[4]Molecular Oncology Research Center, Barretos Cancer Hospital, Barretos, Brazil

Graphic abstract

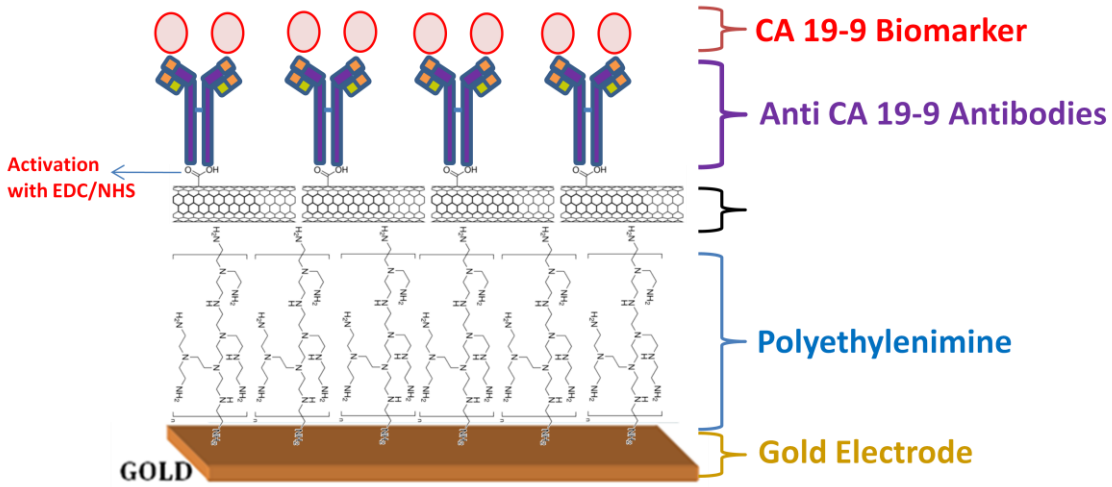

Molecular architectures combining polyethylenimine and carbon nanotubes to detect low concentrations of the CA19-9 biomaker.

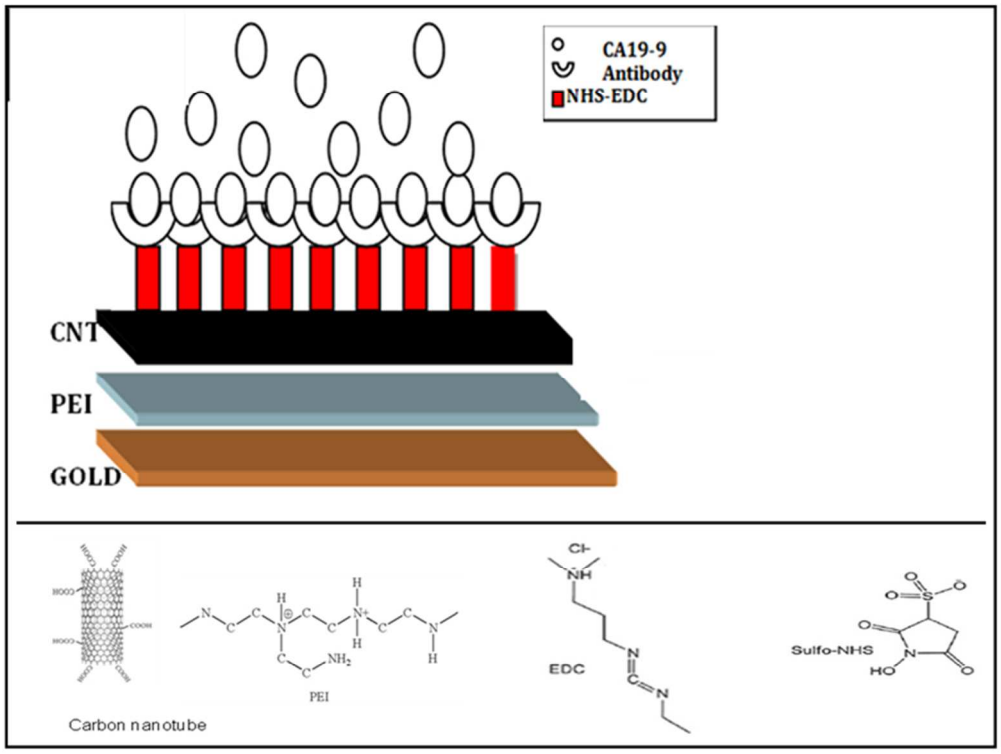

Figure 1: Thin film constructed in a layer-by-layer (LbL) fashion on gold surface using carbon nanotubes (CNTs) and polyethyleneimine (PEI). The carboxylic acid groups on CNTs were activated using NHS-EDC to anchor anti-CA19-9 antibodies on the film surface for specific detection of antigen CA19-9.

212x161mm (96 x 96 DPI)

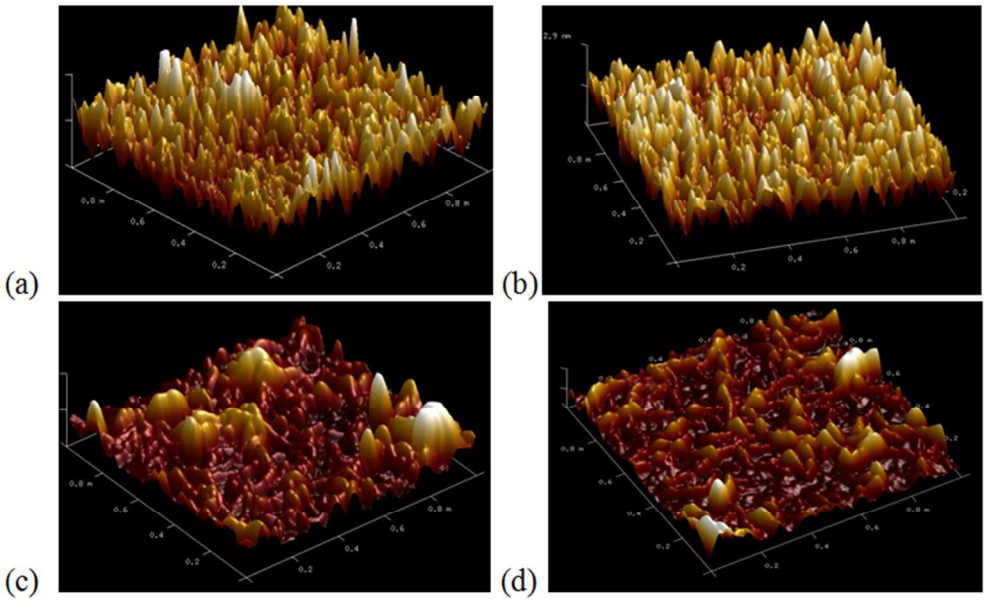

Figure 2. 3-D AFM images showing surface morphology as materials are added layer-by layer in the PEI-CNT film construction. (a) Clean gold surface with roughness 0.943 nm (b) Surface after the deposition of a monolayer of PEI; roughness 0.881 nm (c) Surface after adsorption of CNT; roughness 6.91 nm (d) Surface after adsorption of antibodies (anti-CA19-9); roughness 5.39 nm.

211x131mm (96 x 96 DPI)

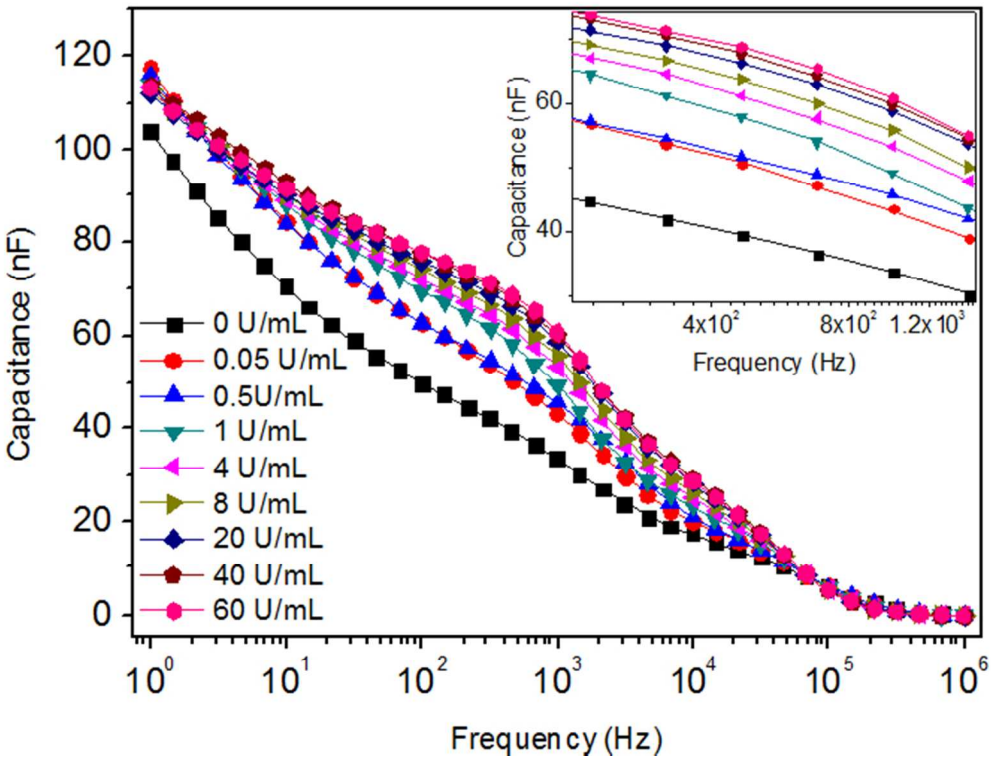

Figure 3: Capacitance versus Frequency spectrum for electrodes modified with PEI-MWCNT films, immersed in PBS solution with different CA19-9 concentrations. The insert shows the data focused between 100 and 1000 Hz.

177x134mm (96 x 96 DPI)

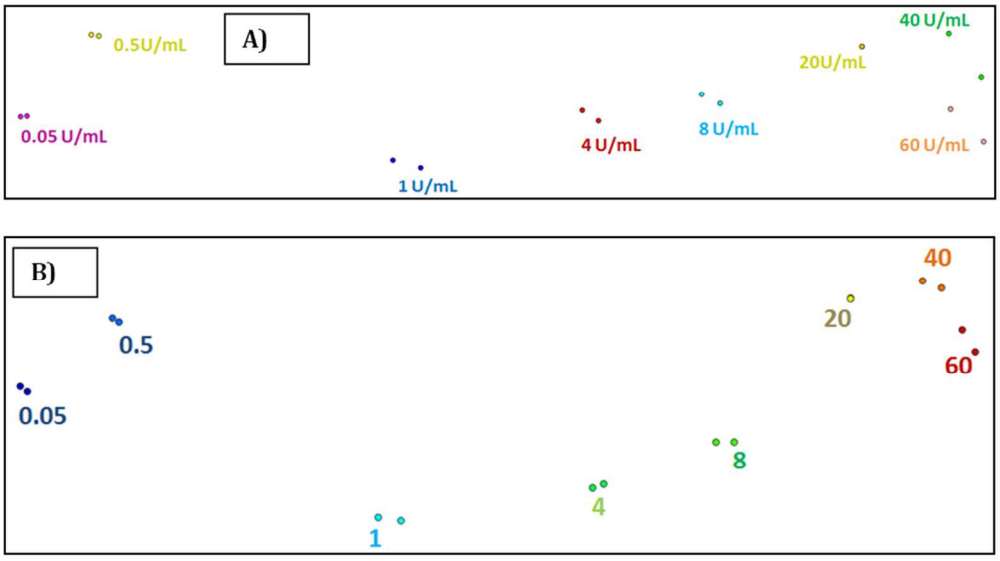

Figure 4. (a) IDMAP of capacitance vs. frequency data of CA19-9 biomarker diluted in PBS solution. (b) IDMAP of capacitance x frequency data of CA19-9 biomarker for 10 selected frequencies. Each dot represents the spectrum for the corresponding concentration. The axes are not labelled because what matters in the plot is the relative distance between data points.

257x144mm (96 x 96 DPI)

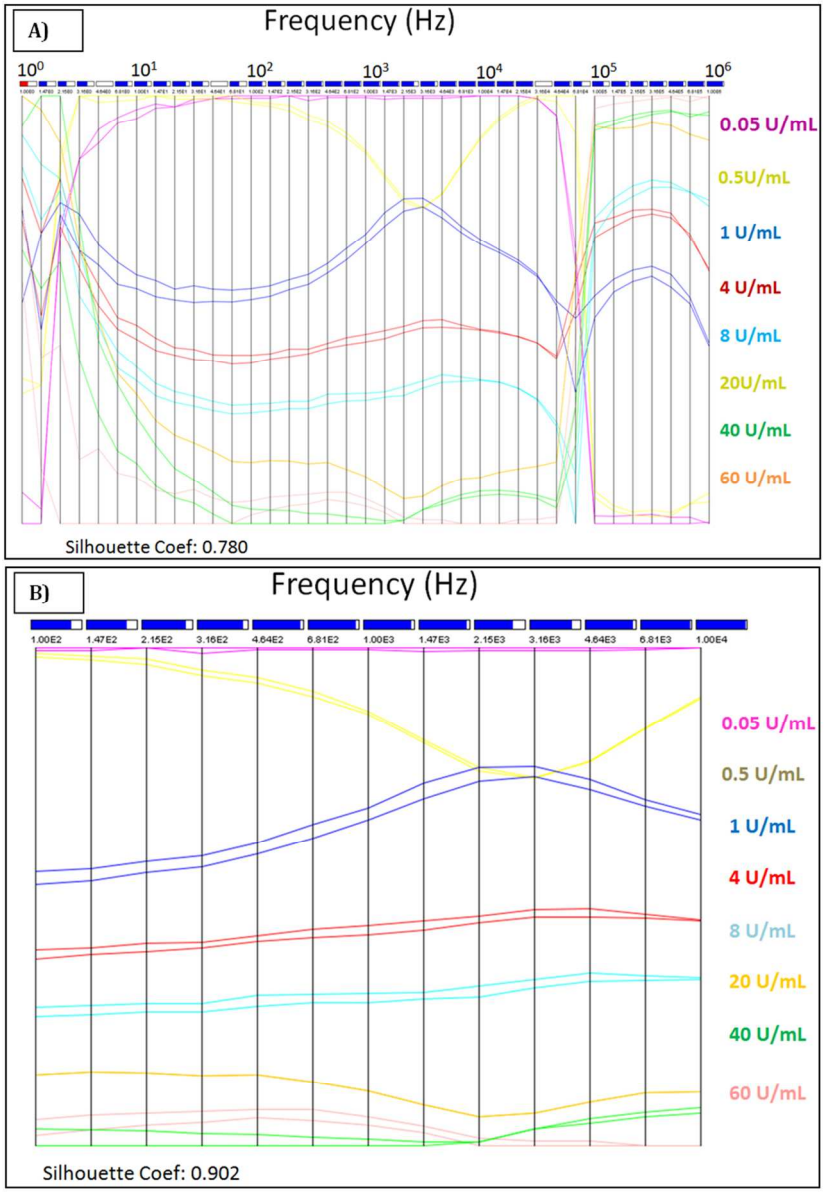

Figure 5: (a) Parallel coordinates graph obtained from capacitance x frequency spectra of different CA19-9 concentrations in commercial samples. (b) Parallel coordinates graph obtained from capacitance x frequency spectra for 10 selected frequencies. The x-axis corresponds to the frequency while the y-axis brings normalized capacitance values. The blue boxes indicate that the region of intermediate frequencies, between 100-10000 Hz, is more suitable to distinguish the samples.

257x375mm (96 x 96 DPI)

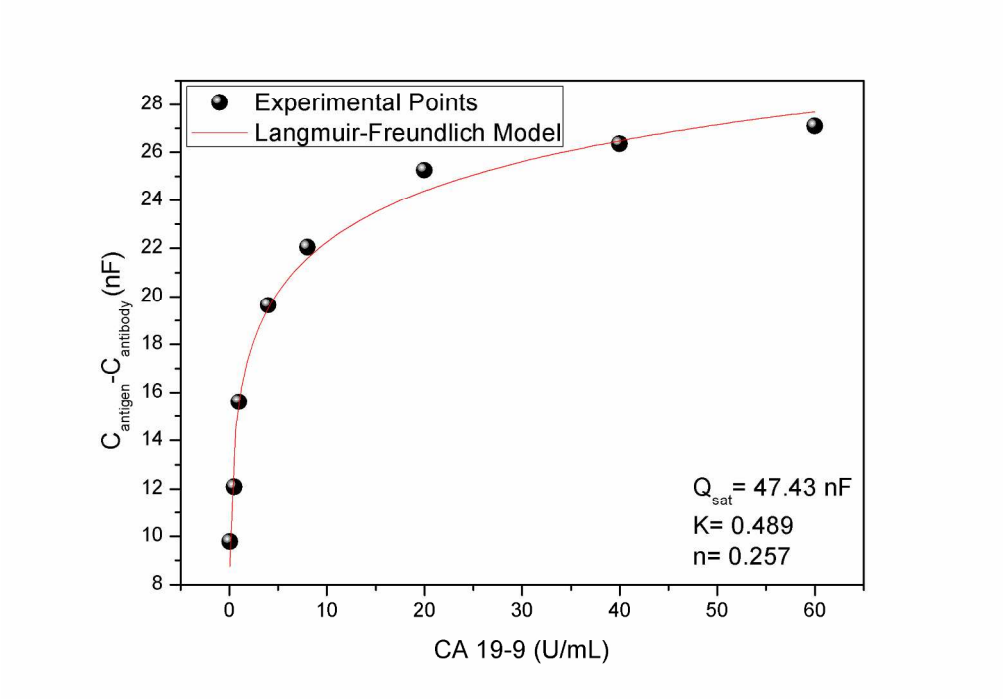

Figure 6. Relative capacitance showing capacitance change upon adsorption of CA19-9. The adsorption behaviour is modelled by a Langmuir-Freundlich isotherm (solid line).

215x151mm (300 x 300 DPI)

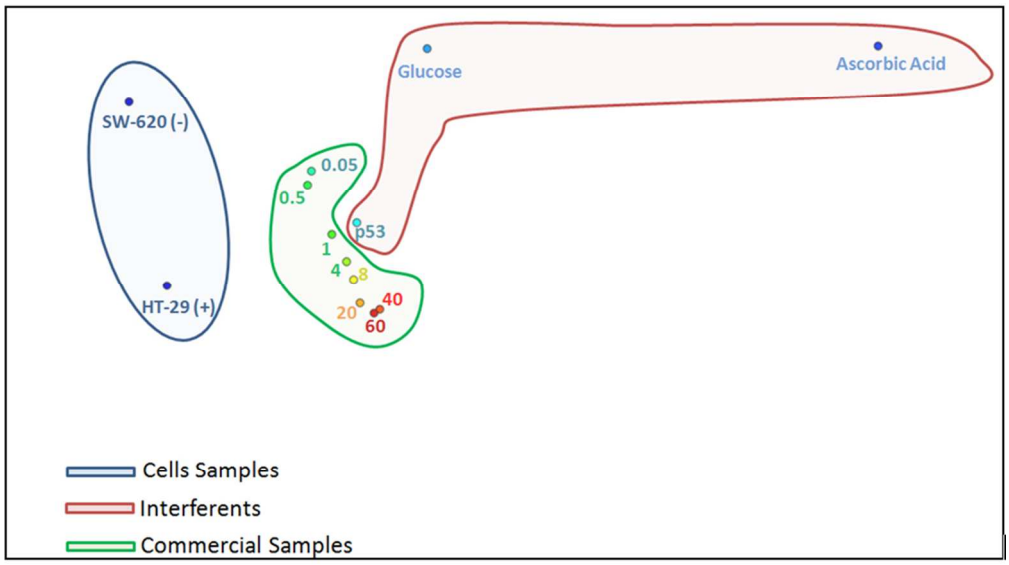

Figure 7: IDMAP of capacitance x frequency spectra of two supernatants cells samples HT-29 and SW-620 (blue region), three interferents (red region) and commercial samples (green region), indicating absence of false positives and the presence of CA 19-9 in HT-29 cell supernatants. As in Figure 4, the axes are not labelled.

256x143mm (96 x 96 DPI)

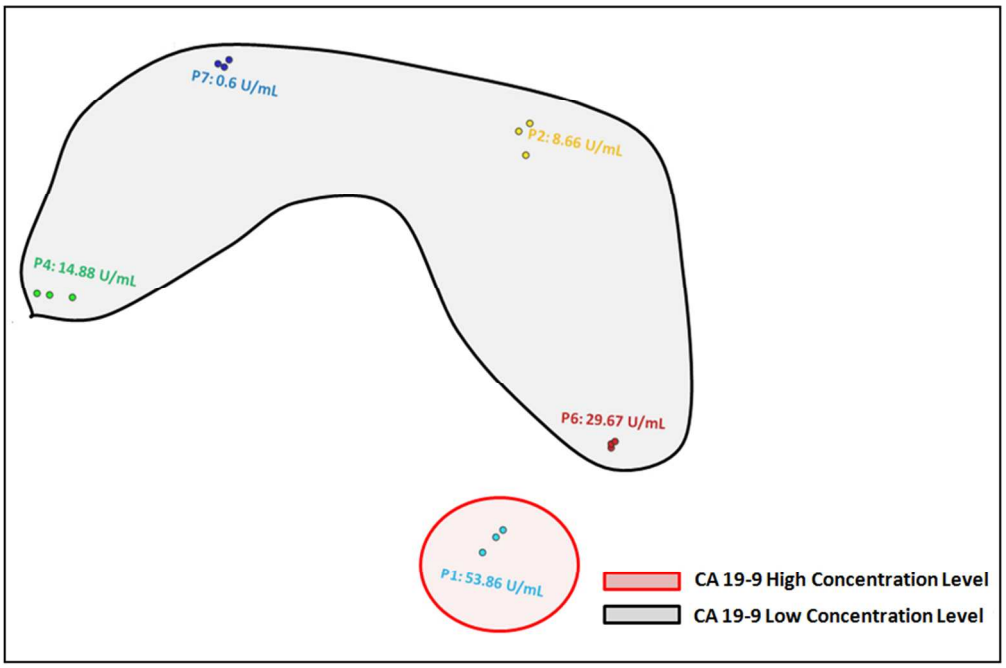

Figure 8: IDMAP obtained from the capacitance x frequency curves of 5 serum samples from patients from Barretos Cancer Hospital (Ethics Committee number 1.447.041, Brazil). As in Figures 4 and 7 the axes are not labelled.

256x169mm (96 x 96 DPI)

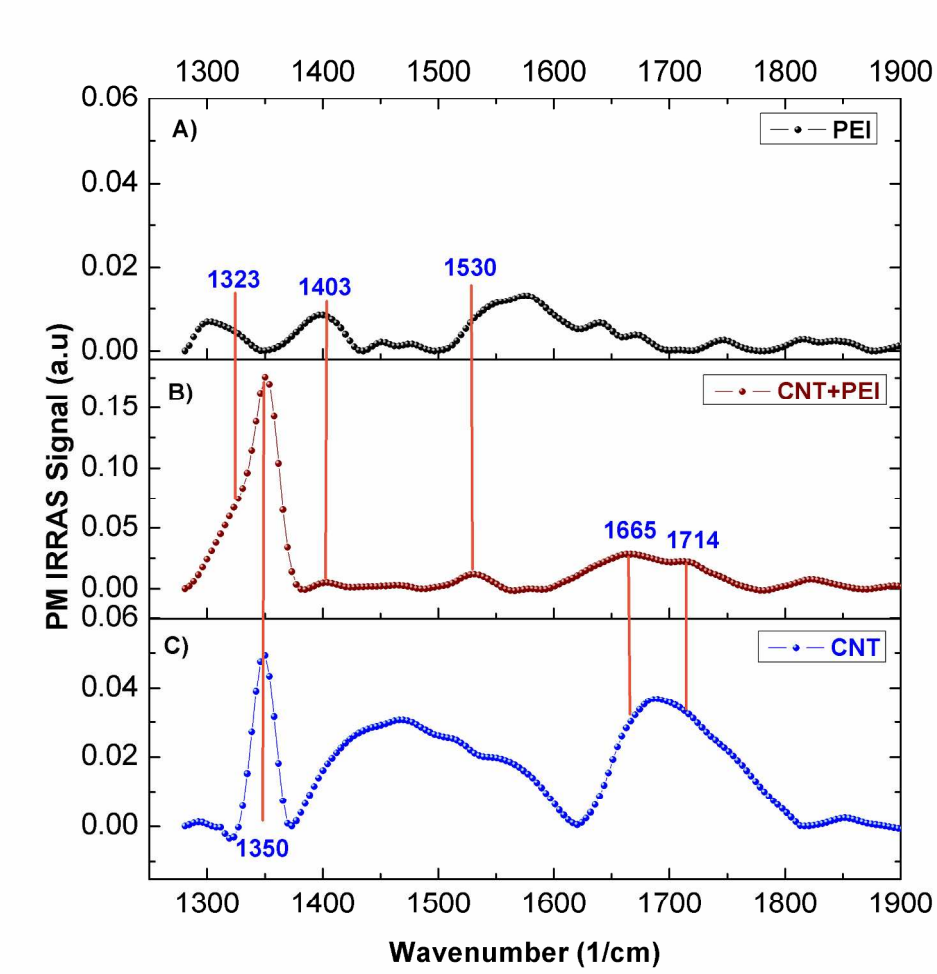

Figure 9: PM-IRRAS signal of the PEI-CNT biosensor in (1300-1900)〖cm〗^(-1) infrared frequency region.

215x215mm (300 x 300 DPI)

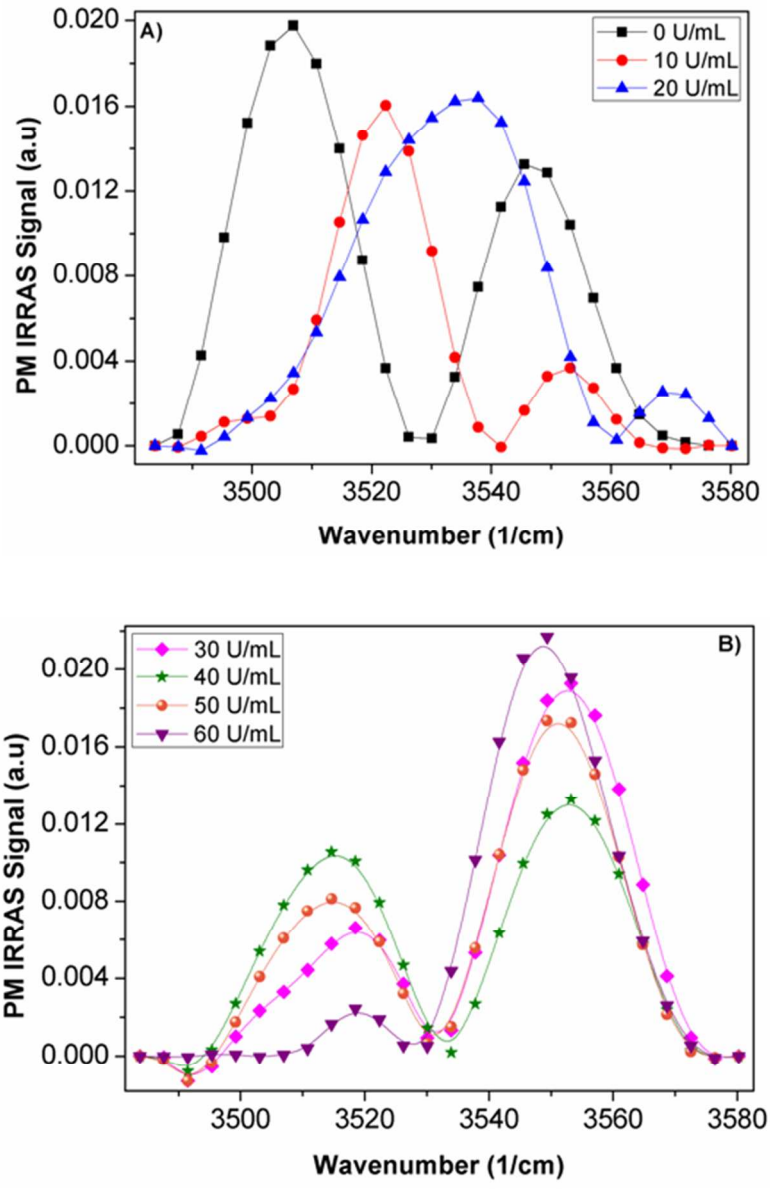

Figure 10: PM IRRAS spectra of adsorption CA 19-9 biomarkers in active layer immobilized in carbon nanotubes matrix: (a) Spectra between 0-20 U/mL (b) Spectra between 30 and 60 U/mL.

142x216mm (96 x 96 DPI)

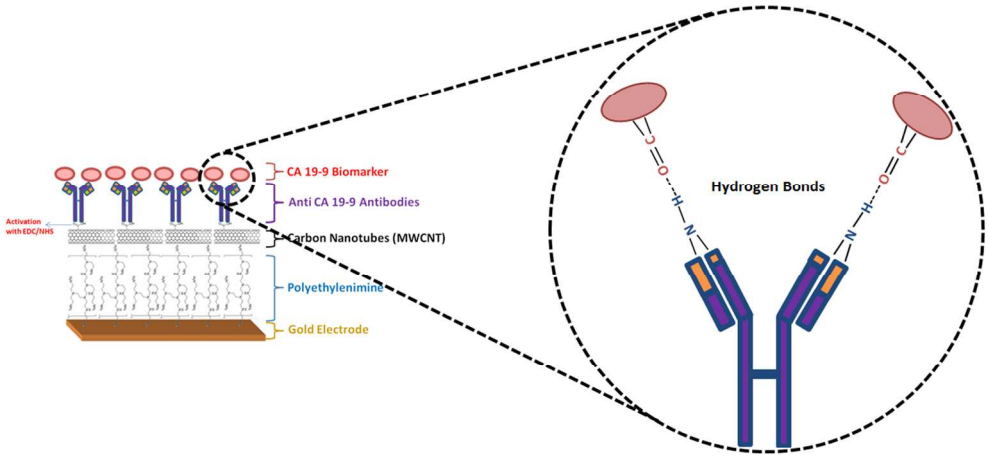

Figure 11. The figure depicts schematically the interactions taking place between antibodies and antigens, which are responsible for the sensing mechanisms. The whole architecture of the biosensor is represented. Specificity of the antigen-antibody interactions is warranted by the surface shape of the topmost layer containing the anti-CA19-9 antibodies. In the zoomed figure, H-bonds are shown which lead to shifts in NH and amide bands in the PM-IRRAS spectra.

330x148mm (96 x 96 DPI)